

Computation of Cole-Cole parameters from IP data

Yuval*, Douglas W. Oldenburg*

ABSTRACT

We develop a process to estimate Cole-Cole parameters from time-domain induced polarization (IP) surveys carried out over a nonuniform earth. The recovery of parameters takes the following steps. We first divide the earth into rectangular cells and assume that the Cole-Cole decay parameters η_0 , τ , and c are constant in each cell. Apparent chargeability data measured at times t_k after the cessation of the input current are inverted using a 2-D inversion algorithm to recover the intrinsic chargeability structure $\eta(t_k; x, z)$ for $k = 1, L$, where L is the number of time channels measured. When carrying out this inversion, it is necessary to introduce a normalization criterion so that the inversion outputs from the different time channels can be meaningfully combined. The L chargeability structures provide L estimates of the chargeability decay curve for each cell. The desired intrinsic Cole-Cole parameters are recovered from these decay curves using a very fast simulated annealing (VFSA) algorithm. Application of the process in all cells provides interpretation maps of $\eta_0(x, z)$, $\tau(x, z)$, and $c(x, z)$. Our analysis is demonstrated on a synthetic example and is implemented on a field data set. The application of the process to field data yields reasonable results.

INTRODUCTION

Induced polarization (IP) is a relaxation phenomenon of polarized charges and can be observed in both frequency- and time-domain experiments. The variability of the nature of the relaxation was recognized by the early researchers in the 1950s; since then, attempts have been made to study and understand the causes. Zonge and Wynn (1975) demonstrated several applications of the complex resistivity method to separate the responses of economic polarized targets from other anomalies. Pelton et al. (1978) investigated the applicability of modeling

the IP phenomenon using the Cole-Cole relaxation model. The transfer function of the simple Cole-Cole model is

$$Z(\omega) = R_0 \left[1 - \eta_0 \left(1 - \frac{1}{1 + (i\omega\tau)^c} \right) \right], \quad (1)$$

where R_0 is the low frequency resistance, ω is the angular frequency, η_0 is the intrinsic chargeability as defined in Siegel (1959), τ is a time constant that characterizes the decay and c is a constant which controls the frequency dependence and is bounded between the values of 0.0 and 1.0. Pelton et al. (1978) found that complex resistivity data can be sensibly modeled by a single or double Cole-Cole model. Their field data were obtained by a dipole-dipole array with 1-m spacing. Because of the small spacing of the electrode array, it is likely that the earth could be regarded as uniform, and hence the recorded, or apparent, IP data could be analyzed directly to estimate the Cole-Cole parameters. They concluded that the resultant Cole-Cole parameters can be useful in mineral discrimination and removal of EM coupling. Pelton et al. used a Marquardt least-squares inversion to fit Cole-Cole parameters to their field and laboratory data. Johnson (1990) suggested a somewhat different inversion method to recover the Cole-Cole parameters from routine time-domain IP measurements.

It is a common practice to recover Cole-Cole parameters from apparent IP data. The difficulty arises when the intrinsic IP chargeability of the earth varies spatially, and hence the apparent IP data result from mixing of the intrinsic responses (Soininen, 1985). Recovery of Cole-Cole parameters from such data can be made, but the relation between these recovered apparent parameters and the intrinsic Cole-Cole parameters is not clear. In this paper, we suggest an alternative approach that enables recovery of the intrinsic Cole-Cole parameters from field data. We first invert the apparent chargeabilities associated with each time channel to recover an estimate of the intrinsic chargeability as a function of spatial position that is associated with that time. Inversion results are combined to form an intrinsic decay curve for each cell. The Cole-Cole parameters that provide a best fit to the decay curves are found by carrying out a parametric inversion using a very fast simulated annealing

Manuscript received by the Editor September 5, 1995; revised manuscript received July 17, 1996.

*U.B.C.-Geophysical Inversion Facility, Department of Earth and Ocean Sciences, University of British Columbia, Vancouver, British Columbia, Canada V6T 1Z4.

© 1997 Society of Exploration Geophysicists. All rights reserved.

code. The forward modeling of the decay curves are computed using the digital linear filter given in Guptasarma (1982).

Our paper begins with a definition and illustration of the difference between intrinsic and apparent chargeability decay curves. This is followed by a description of the method we use to extract the intrinsic decay curves; it includes a summary of the IP inversion algorithm and a normalization method that is needed to maintain fidelity in the extracted decay curves. Next, we provide background about the simulated annealing inversion algorithm, and then recover intrinsic Cole-Cole parameters for synthetic and field examples. The paper concludes with a discussion.

INTRINSIC AND APPARENT CHARGEABILITY DECAY CURVES

The chargeability η , as defined in Siegel (1959), is a physical property of a medium. Consider a small volume in the earth. In a time-domain survey, polarization charges in the volume are built up when an excitation current is applied. Upon cessation of the current, these charges, and the electric potential, decay with time. The chargeability of the volume element is given by

$$\eta(t) = \frac{\phi(t)}{\phi_\eta}, \tag{2}$$

where $\phi(t)$ is the voltage across the volume after current shutoff at $t = 0$ and ϕ_η is the maximum voltage prior to shutoff which is assumed to have been built up after an infinitely long charging time. Assuming a Cole-Cole model with parameters defined by

equation (1), Pelton et al. (1978) showed that the time-domain intrinsic chargeability curves can be described by

$$\eta(t) = \eta_0 \sum_{n=0}^{\infty} \frac{(-1)^n \left(\frac{t}{\tau}\right)^{nc}}{\Gamma(1 + nc)}, \tag{3}$$

where $\eta_0 = \eta(t = 0)$ and Γ is the Gamma function. All $\eta(t)$ curves begin at η_0 and decay with time. If $c = 1.0$, the expression in equation (3) degenerates to the simple exponential decay $\eta(t) = \eta_0 e^{-t/\tau}$.

An intrinsic chargeability decay curve associated with a particular point in the medium can be inverted to recover the corresponding η_0 , τ , and c . The problem is that $\eta(t)$ is not readily available. In the field, we measure the apparent chargeability $\eta_a(t)$, which is a spatial average of the intrinsic chargeability under the measuring array. In a homogeneous medium the intrinsic and apparent values coincide, but if the medium is heterogeneous the curves differ. Moreover, inversion of the apparent curves can produce only pseudosections of the Cole-Cole parameters, and those cannot provide the shape of the responsive body or give its position in real physical coordinates. This situation is analogous to the difficulties encountered when attempting to interpret pseudosections of apparent chargeability and conductivity.

We demonstrate these points on a synthetic example that we will use throughout the paper. Consider the model in the upper panel of Figure 1. It consists of two chargeable blocks buried in a nonchargeable half-space. The electrical conductivity of

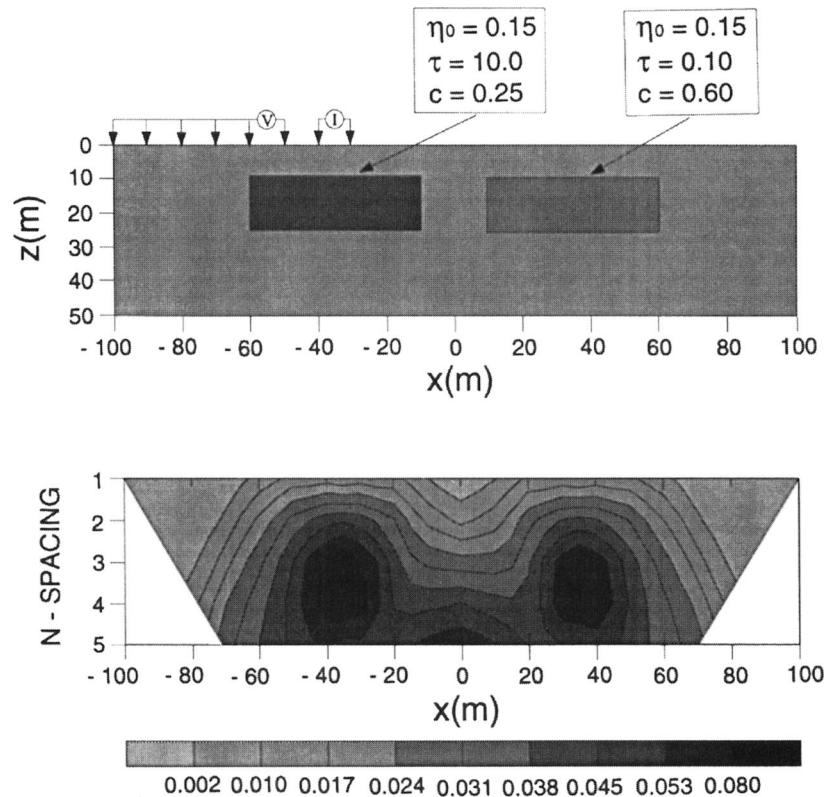


FIG. 1. The synthetic model consists of two chargeable prisms embedded in a nonchargeable, uniform conductive halfspace of 0.01 Sm^{-1} . The pseudosection of the first time-channel data, collected by a dipole-dipole array with $a = 10 \text{ m}$ and $n = 1, 5$, is given at the bottom.

the half-space is 0.01 Sm^{-1} . The 2-D model was divided into 48×22 cells, and the chargeability for each cell at ten discrete time channels was computed using equation (3) and the parameters given in Figure 1. The times of the ten channels are logarithmically spaced in the interval 0.01 to 2.0 s. A dipole-dipole IP survey is carried out with $n = 1, 5$ and $a = 10$ m. In the 2-D model, the chargeability of each cell decays with time. We evaluate this intrinsic chargeability for each time channel and carry out a forward modeling. This results in ten apparent chargeability data sets. The apparent chargeability pseudosection of the data recorded at time channel 1 is given in the lower panel of Figure 1. The two anomalous bodies are observed, but the one on the right appears to have lower amplitude. This is because of the short decay time compared with that of the body on the left.

An apparent chargeability decay curve is available for any current-potential pair. In Figures 2a and 2b, apparent curves are

compared to the original intrinsic decay curves in the blocks. The apparent curves are measured with a current-potential electrode pair located so that the outermost electrodes are above the edges of the blocks. The apparent chargeabilities along these curves are considerably lower than the true intrinsic values, but the shapes of the two curves are similar. In Figure 2c, we show the effects of heterogeneities on the apparent curves. When the measuring array spans both blocks, mixing of the responses create distorted curves that are not compatible with the Cole-Cole model.

In this synthetic example, most of the apparent chargeability curves have characteristic IP decay shapes and can be inverted to recover the apparent Cole-Cole parameters. Using the same inversion methodology that we use to invert intrinsic curves and which will be described in the next section, we inverted these curves and created the apparent η_0 , τ , and c pseudosections shown in Figure 3. Note that we chose to invert the

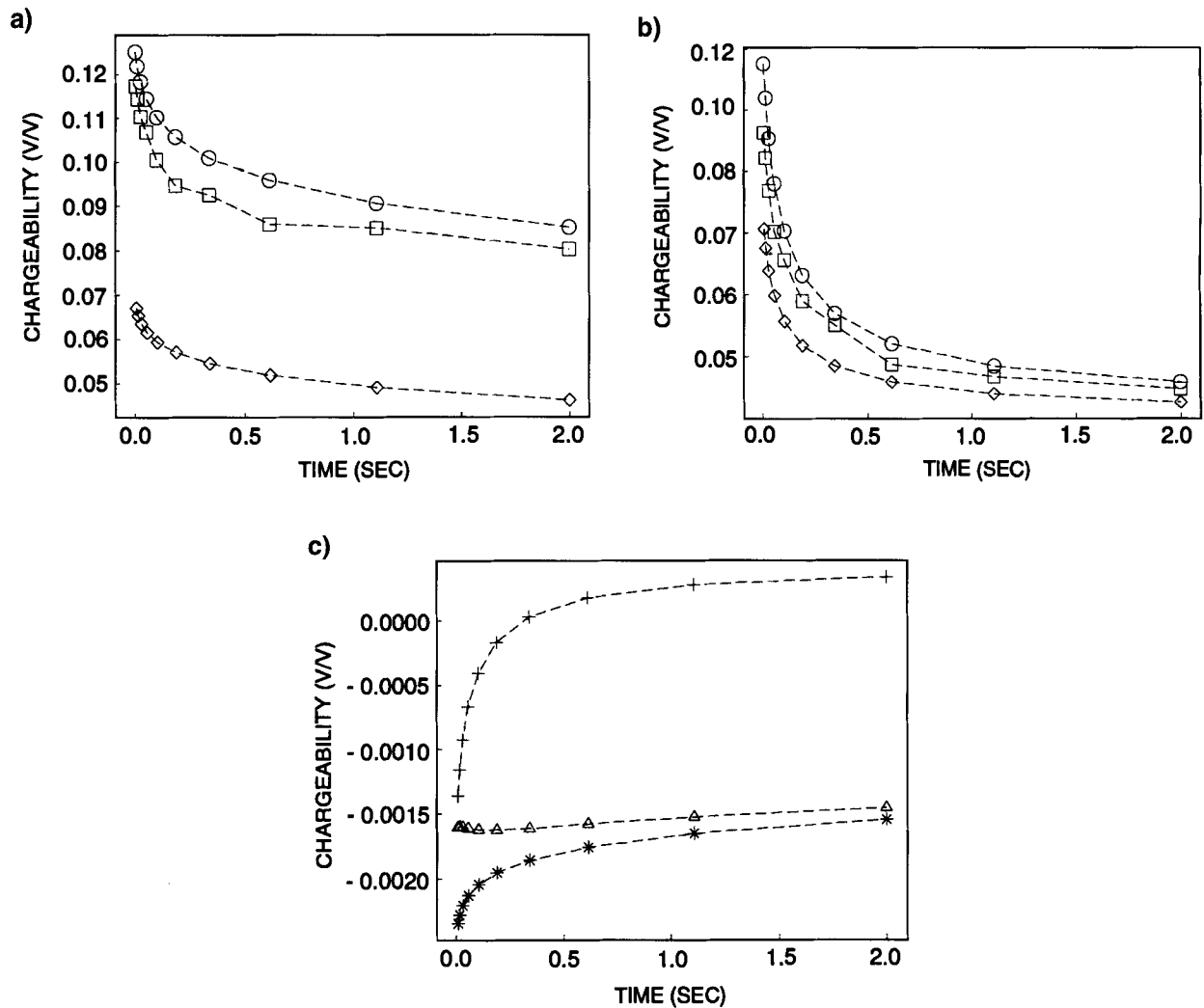


FIG. 2. (a) The circles denote the original intrinsic decay curve corresponding to the chargeable block on the left. An apparent decay curve measured above the block is denoted by diamonds. The current and potential electrodes positions are $(C1, C2, P1, P2) = (-10, -20, -50, -60)$ m, (see Figure 1 for reference). An extracted intrinsic decay curve for a cell at the center of that block is denoted by squares. (b) Corresponding curves for the chargeable block on the right. The current and potential electrodes positions are $(C1, C2, P1, P2) = (60, 50, 20, 10)$ m. (c) Apparent chargeability curves showing the effects of mixing responses. The current and potential electrodes positions for the curves, indicated respectively by $(+, \Delta, *)$, are $(10, 0, -10, -20)$, $(20, 10, 0, -10)$, and $(-60, -70, -80, -90)$ m. These decay curves are not compatible with the single stage Cole-Cole model.

apparent curves prior to contaminating them with noise so inaccuracies in the recovery of the apparent Cole-Cole parameters are only caused by the mixing of intrinsic responses and limitations of the inversion algorithm. The apparent η_0 pseudosection shows three distinctive highs. Two of them are symmetrical and correspond to the chargeable blocks. The third high in the middle of the section, and at larger n-spacings, is purely an artifact of mixing the responses of the two blocks. The highest apparent η_0 value does not exceed 0.09 V/V; this is substantially less than the true value of 0.15 for the two blocks. The pseudosection of apparent τ shows two distinct areas of uniform values.

Although values are representative of the true τ values for the blocks, there is no indication of the actual physical shape of the anomalous bodies. The pseudosection for apparent c shows values of about 0.6 on the right and about 0.25 on the left. These are correspondingly the c values of the right and left blocks, but again there is no information about the actual shapes of the responsive bodies. The pseudosections for τ and c have spuriously large values in regions between, and at the edges, of the blocks. These artifacts, which are caused by mixing and geometrical effects, inhibit visual interpretation of the data.

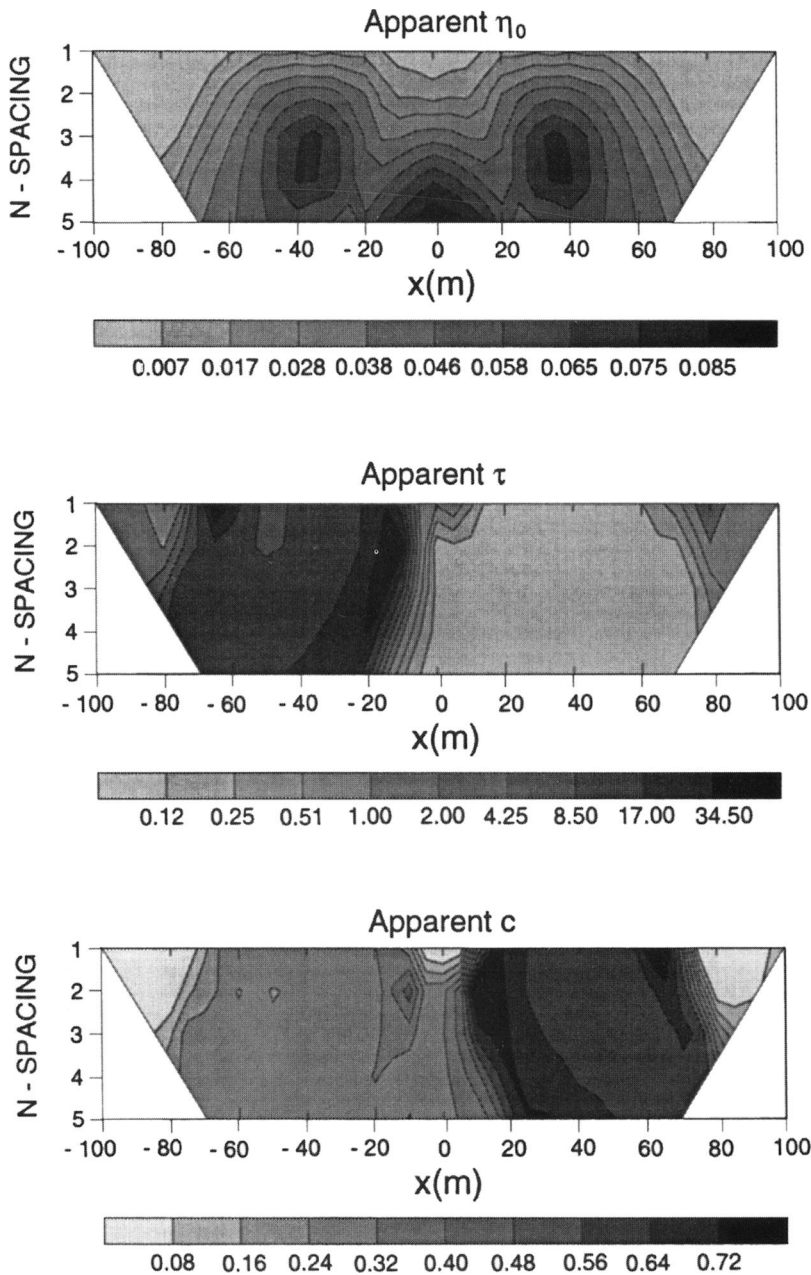


FIG. 3. Pseudosections of the recovered Cole-Cole parameters for the synthetic example.

EXTRACTION OF INTRINSIC IP DECAY CURVES FROM THE DATA

The linearized relationship between the apparent chargeability data and the chargeability model is assumed to be

$$d_i^k = \sum_{j=1}^M J_{ij} \eta_j^k(\eta_{0j}, \tau_j, c_j); \quad i = 1, N, \quad k = 1, L \quad (4)$$

where J_{ij} is an element of the sensitivity matrix, M is the number of cells, N is the number of apparent chargeability data for each time channel, k denotes the time channel, and L is the number of time channels. The goal of recovering the intrinsic Cole-Cole parameters can be approached in two ways. The first would be to set up a full nonlinear inversion to solve for the $3M$ parameters for the $L \times N$ data. An alternative method is to invert data from each time channel separately to recover the distribution of the intrinsic chargeability for that time, collect the results to form the intrinsic IP decay curve for each cell, and then carry out a nonlinear parametric inversion to recover the Cole-Cole parameters for each cell. In this paper, we adopt the latter approach.

The inversion of IP data for any time channel is carried out using the methodology given in Oldenburg and Li (1994). The IP inverse problem is posed as an optimization problem where an objective function,

$$\psi_m(\eta) = \|W_m \eta\|^2, \quad (5)$$

is minimized subject to the data constraints

$$\psi_d(d, d^{obs}) = \|W_d(d - d^{obs})\|^2 = \psi_d^*. \quad (6)$$

In equations (5) and (6), η is the sought model, d^{obs} is the observed apparent chargeability data, d is the predicted apparent chargeability data forward modeled with η using equation (4), W_m and W_d are weighting matrices, and ψ_d^* is the desired misfit. The final model achieved by the inversion has manifestations of the chosen objective function that is embedded in the W_m matrix. It also depends on the assumed errors in the observed data that are given in the W_d matrix and on the final misfit ψ_d^* . Because our goal is to extract intrinsic decay curves from the output of L IP inversions, it is essential that all of the inversions are carried out consistently. First, this requires that the model objective function be the same for each inversion. More problematic is the assignment of errors and the choice of the target misfit for each of the inversions. Here, we choose W_d to be $\text{diag}[1/\epsilon_i]$ where ϵ_i is the assumed standard deviation of the data. If the true errors on the data are Gaussian and have standard deviations equal to the assigned values, then the inversion should be carried out with a target misfit of $\psi_d^* \approx N$. In our synthetic example, we added random Gaussian noise equaling 5% of the average value of the data set prior to the IP inversion.

Inverting data from all time channels results in L chargeability models. In Figure 4, we present recovered models corresponding to the first, fifth, and tenth time channels. The chargeable blocks are visible in each inverted model, and the amplitude of the recovered chargeabilities decreases with increasing time as it should. For any cell in the 2-D model domain, we can extract the chargeabilities obtained from the individual inversions and thereby generate an intrinsic chargeability decay curve for that cell. In Figures 2a and 2b, we compare

extracted intrinsic curves at cells in the middle of the blocks to the true intrinsic curves. The extracted intrinsic curves are in much better agreement with the true curves than are the apparent curves extracted directly from the field data.

To conclude this section, we turn to an essential aspect that needs to be considered when field data are processed. In the synthetic example, we knew the standard deviation of the Gaussian noise and each data set was inverted so that the final misfit was equal to the expected value of N . In field data sets, the errors are unknown and, if the inversions are carried out so that the final misfits are identical, then some data sets will be overfit and others will be underfit. This will produce distortions in the extracted decay curves because overfitting the data generates a model with excessive structure, whereas underfitting produces chargeability models with too little structure. To overcome this difficulty, we take the following approach. We ascribe errors for $d^{obs(1)}$, data from the first time channel, and carry out the inversion to produce a chargeability model $\eta^{(1)}$. Let $\psi_d^{*(1)}$ denote the achieved target misfit. Now consider the inversion of data from the k th time channel. Since the data errors in the k th channel are likely different from those in the first channel, $\psi_d^{*(1)}$ should not be used as a target misfit. Rather, we adjust the misfit until we satisfy

$$\|\eta^{(k)}\| = \frac{\|d^{obs(k)}\|}{\|d^{obs(1)}\|} \|\eta^{(1)}\| \equiv f^{(k)} \|\eta^{(1)}\| \quad (7)$$

or

$$\|d^{(k)}\| = \frac{\|d^{obs(k)}\|}{\|d^{obs(1)}\|} \|d^{(1)}\| \equiv f^{(k)} \|d^{(1)}\|, \quad (8)$$

where $\eta^{(k)}$ is the recovered model of the k th time channel, $d^{(k)}$ are the predicted data, and $\|\cdot\|$ indicates the ℓ_1 norm of a vector.

The rationale for using equations (7) and (8) to normalize the inversions follows from considering an earth in which the (τ, c) parameters are uniform. In such a case, for every cell $\eta_j(t_k) \equiv \eta_j^{(k)} = f^{(k)} \eta_j^{(1)}$, where $f^{(k)}$ is a constant which depends upon (τ, c) and the times t_1 and t_k . It follows that $\|\eta^{(k)}\| = f^{(k)} \|\eta^{(1)}\|$. The constant $f^{(k)}$ is unknown, but it can be evaluated from the data. The relationship between the data and chargeability is linear; hence, for the i th datum, $d_i^{(k)} = f^{(k)} d_i^{(1)}$ and also $\|d^{(k)}\| = f^{(k)} \|d^{(1)}\|$. The same relationship is true for the observed data and, hence, the desired constant is estimated as

$$f^{(k)} = \frac{\|d^{obs(k)}\|}{\|d^{obs(1)}\|}. \quad (9)$$

To obtain some insight as to whether equation (7) or (8) is more valid under conditions when the Cole-Cole parameters vary spatially, we return to the synthetic example. There, we knew the standard deviations of the data and used a misfit criterion of $\psi_d^* = N$. This provided L models $\eta^{(k)}$, and multiplication of those models by the sensitivity matrix provided L predicted data $d^{(k)}$. Thus all normed quantities in equations (7) and (8) can be calculated. The validity of equations (7) and (8) can be evaluated by dividing each equation by its right-hand side. The ideal result is unity. Table 1 presents the ratios for time channels $k = 2, 10$. The two methods of normalization are seen to be very

similar with equation (8) having a slight edge. Henceforth, we use that equation to normalize field data inversions.

SIMULATED ANNEALING INVERSION OF IP DECAY CURVES

The inversions of the individual time channels provide L estimates $\eta^{ext}(t_k)$ of an intrinsic decay curve $\eta(t)$ for each cell. The desired Cole-Cole parameters can be recovered from these curves by carrying out a parametric inversion. An important

aspect is the choice of error criterion. Each datum $\eta^{ext}(t_k)$ is the output of an inversion program in which there are many more model parameters than IP data. The output is controlled by the model objective function that is minimized and by the choice of desired misfit. These aspects alone prevent us from assigning an error to any datum. Other factors such as non-Gaussian noise on the field data, inadequate cellularization of the earth model, and representation of a 3-D earth with a 2-D algorithm cause additional uncertainty in the recovered models, and we must

Table 1. Numerical evaluation of equations (7) and (8) to determine which equation is better suited to normalize the data when inverting many time channels.*

Method	TC 2	TC 3	TC 4	TC 5	TC 6	TC 7	TC 8	TC 9	TC 10
Eq 7	1.0070	1.0085	1.0078	1.0023	1.0072	1.0069	1.0416	1.0021	0.9870
Eq 8	1.0004	1.0001	1.0006	1.0011	1.0007	1.0029	1.0011	1.0037	1.0035

*The observed and predicted data, and the chargeability models needed to evaluate the quantities in equations (7) and (8), are obtained from the synthetic model of two chargeable prisms buried in a uniformly conducting halfspace. The desired ratio for each time channel inversion is unity.

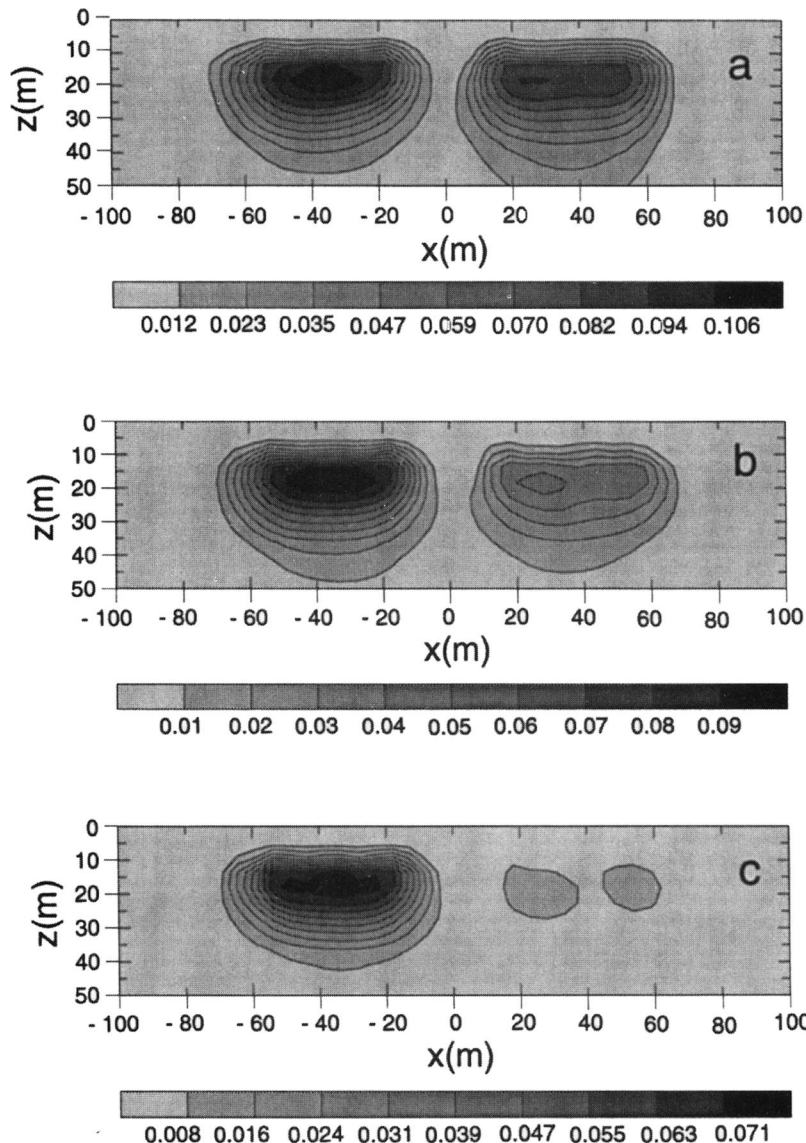


FIG. 4. Chargeability models recovered by inverting data from the (a) first, (b) fifth, and (c) tenth time channels.

conclude that the error on $\eta^{ext}(t_k)$ is unknown. Our approach is to search for a set of Cole-Cole parameters which fit the data as well as possible. A general misfit function considered here has the form

$$\phi_d = \|W_d(\eta^{ext} - \eta^p)\|_n, \quad (10)$$

where η^p are the predicted data. In equation (10), the weighting matrix W_d could be the identity, if all data had approximately the same error, or W_d could be a diagonal matrix whose k th element is $1.0/\eta^{ext}(t_k)$, if relative errors are more appropriate. The value of n , although potentially any positive number, is taken as 1 or 2. If $n = 1$, then ϕ_d becomes an ℓ_1 norm and sensitivity to outliers is reduced. If $n = 2$, ϕ_d is the usual ℓ_2 or least-squares norm. In addition one can use $\log[\eta^{ext}(t_k)]$ as data, but this has the same effect as using relative errors. The difficulty or trying to estimate the errors is illustrated in Figure 2, where the true and extracted decay curves for a cell at the center of each chargeable prism are plotted. The extracted curves lie below the true curves, and the difference is greater for the left block than for the right block. If the differences between the two curves is regarded as "error," then the errors are biased and non-Gaussian. But biased data may not be completely deleterious. If differences between the curves can be accounted for by a multiplicative constant, then the correct (τ, c) values can still be obtained, although η_0 will be in error by the multiplicative factor. Differences which cannot be accounted for by scaling will affect the recovered values of all of the Cole-Cole parameters. The choice of which misfit norm to use is thus likely to be problem dependent. Some important criteria include the expected values of τ and c , decisions about how well outliers should be fit, and whether a better fit to data at early times or later times is desired. We offer no universal answer, but we have experimented with different choices of misfit function on synthetic and field data. As an illustration, we invert the true and extracted intrinsic decay curves in Figure 2 with four choices of ϕ_d obtained by setting $n = 1$ and 2 and setting $W_d = I$ and $W_d = \text{diag}\{1/\eta^{ext}\}$. The results are presented in Table 2. The recovered parameters are reasonably similar for different choices of misfit, but overall, the combination ($n = 1, W_d = I$) might be considered superior. Trials with other data sets also show this similarity in results. For historical reasons, we use the least-squares misfit norm obtained by setting $W_d = I$ and $n = 2$ in equation (10).

Solving the parametric inverse problem requires the ability to carry out forward modeling. Equation (3) forms the formal Cole-Cole forward modeling of the IP response to a

step function of applied current. Unfortunately, the infinite sum in expression (3) converges very slowly for large values of t/τ ; thus we carried out our forward computations of the step response using the method given by Guptasarma (1982). Guptasarma designed a digital linear filter that transforms the frequency-domain response of polarized ground into the time-domain response. The computation is easy to carry out, and the results are accurate to better than 1% error. It is also very fast. For a step turnoff about 10000, forward modelings of a 10-point curve can be carried out in less than a minute on a Sun SPARC 10 machine. If the input in the field survey is a square wave, $(+, 0, -, 0, \dots)$, of impressed current, then the forward modeling of this pulse train response requires a superposition of the series of positive and negative step responses (Madden and Cantwell, 1967). The infinite pulse train response is calculated by summing the terms of the alternating series using Euler's transformation (Press et. al., 1992) to accelerate the convergence.

To solve the parametric inverse problem, we have chosen simulated annealing (SA), which is a method for global optimization first proposed in Metropolis et al. (1953). The reasons for using SA rather than a linearized algorithm are threefold. First, we wanted to have an algorithm that could easily handle different misfit objective functions. Second, linearized techniques such as Marquardt algorithms can get trapped in local minima, whereas SA algorithms have the potential for finding the global minimum of an objective function. Third, incorporation of a priori knowledge to reduce the nonuniqueness of the solution is natural and easy to implement in the SA algorithm. We use a very fast simulated annealing (VFSA) algorithm, which incorporates a different probability distribution for the random walk in model space and is faster in achieving the equilibrium state than the classic SA. The interested reader is referred to Kirkpatrick et al. (1983) and van Laarhoven and Aarts (1988) for further details about the SA method, and to Ingber (1989) for details of the VFSA method.

Convergence of a simulated annealing algorithm depends upon the starting temperature, the schedule for decreasing the temperature and the number of trials at each temperature level. These can be set up by using VFSA to invert synthetic data using the time channels that are available from the survey and values of τ and c which span the range of these parameters for the area of interest. Despite the fact that SA is theoretically capable of finding a global minimum of a function, it is unlikely with a finite number of forward modelings that this will happen. We have, therefore, inverted each decay curve a number of times and taken either the smallest misfit or the average of

Table 2. Cole-Cole parameter inversion results of the curves in Figure 2 using different measures of misfit obtained by altering W_d and n in equation (10)*.

	$n = 1, W_d = I$			$n = 1, W_d = 1/\eta^{obs}$			$n = 2, W_d = I$			$n = 2, W_d = 1/\eta^{obs}$		
	η_0	τ	c	η_0	τ	c	η_0	τ	c	η_0	τ	c
A	0.163	9.211	0.248	0.171	6.992	0.221	0.151	9.843	0.260	0.162	6.290	0.215
B	0.153	5.593	0.224	0.157	5.940	0.244	0.156	4.387	0.208	0.148	6.357	0.224
C	0.148	0.103	0.604	0.146	0.108	0.606	0.149	0.103	0.602	0.150	0.099	0.599
D	0.118	0.111	0.610	0.109	0.148	0.640	0.116	0.120	0.616	0.115	0.123	0.625

*A and B show, respectively, the results of inverting the true and extracted curves in the left block. The true parameters are $(\eta_0, \tau, c) = (0.15, 10.0, 0.25)$. C and D show respectively the results of inverting the true and extracted curves in the right block. The true parameters are $(\eta_0, \tau, c) = (0.15, 0.1, 0.60)$.

the parameters for all runs. The latter option, although not completely justifiable, does produce somewhat better results when the data are contaminated with errors.

SYNTHETIC EXAMPLE RESULTS

We have inverted the decay curve for each cell in the synthetic model. Spatial maps of the Cole-Cole parameters are given in Figure 5. The map of $\eta_0(x, z)$ displays the locations of the two chargeable blocks. The recovered values of η_0 in the left block reach the true value of 0.15, but those in the right block have a maximum of 0.13. Nonzero chargeabilities outside the boundaries of the true blocks exist because the IP inversions produce smooth chargeability models that fit the data (see Figure 4). As a consequence, the recovered value of η_0 gradually decreases to zero away from the true blocks. As displayed in Figure 4, an inversion of IP data for a specific time channel

yields chargeabilities that depend upon the time channel and the intrinsic Cole-Cole parameters. The procedure used to obtain the chargeability in Figure 5 overcomes this and produces estimates of the true intrinsic chargeability. From the second panel in Figure 5, we observe that the recovered τ values for the left block are in the range (2.5, 40.0) and those for the right block are (0.09, 0.13). These numbers are in moderately good agreement with the true values if one considers that τ spans a few orders of magnitude and is treated as a logarithmic parameter in the inversion. Importantly, the variance in τ values is narrow enough to enable a clear distinction between the time constants of the blocks to be made. The last panel in Figure 5 is the recovered c section. The c values in the right block tend to be slightly higher than the original value of 0.60 and vary between 0.58 and 0.65. The values in the left block concentrate around the original value of 0.25, but with a larger variance of

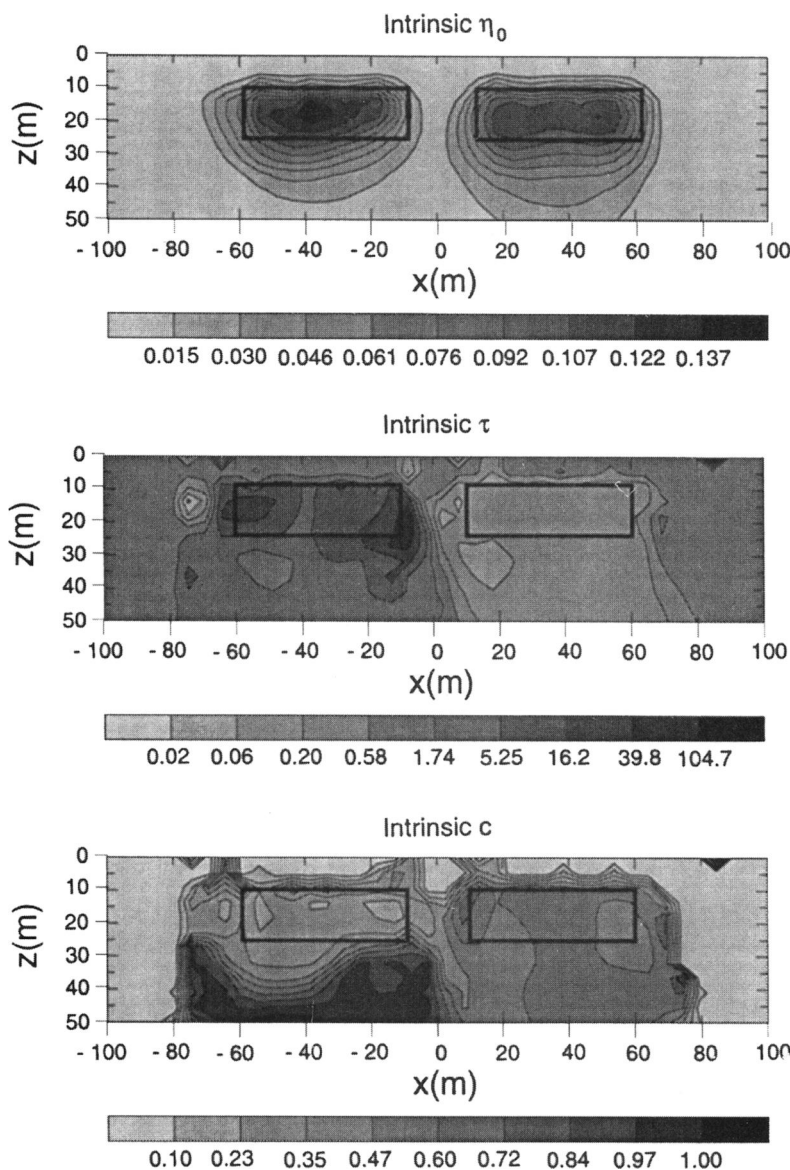


FIG. 5. (a) Recovered intrinsic Cole-Cole parameters in the synthetic example. The rectangular black frames denote the actual physical locations of the original blocks.

0.17–0.32. Again, there is clear distinction between the values of the parameter of the two blocks.

The τ and c panels in Figure 5 display a great deal of structure away from the blocks, but this is not meaningful. If the amplitude of a decay curve is too small, or equivalently if η_0 is too small, it is not likely that recovered estimates of τ and c will be reliable. Interpretation of τ and c sections, therefore, needs to be carried out in conjunction with the η_0 section. This can be done by thresholding the τ and c panels in accordance with the values of η_0 . Neglecting all values of τ and c associated with cells whose $\eta_0 < 0.05$ would be reasonable for this example. For the plots in Figure 5, we had chosen a threshold of $\eta_0 = 0.001$. This artificially low value provides insight about how the smooth model inversions extend values of Cole-Cole parameters away from discrete blocks. The same inversion results, but now thresholded to a more realistic value of 0.05, are shown in Figure 6.

The comparison of the intrinsic η_0 , τ , and c sections in Figure 6 with the corresponding apparent sections of Figure 3 clearly shows the advantages of our method. We reconstruct the anomalies of the Cole-Cole parameters in real physical coordinates and with reasonable accuracy. The map of $\eta_0(x, z)$ indicates the depth of burial and the width of the blocks, and the high chargeability artifact between the prisms has been removed. Although noise was added to the apparent chargeability data prior to the IP inversions, the recovered values of τ and c for the blocks are close to their true values.

FIELD DATA EXAMPLE

The field data example is a pole-dipole survey, $n = 1, 6$ and $a = 25$ m. A 2-s on/off square wave current was used in data collection. The chargeability data were recorded in 11 time channels, the midtimes of which are (0.06, 0.09, 0.13, 0.19, 0.27, 0.38, 0.52, 0.705, 0.935, 1.23, 1.59) s. The data were taken over

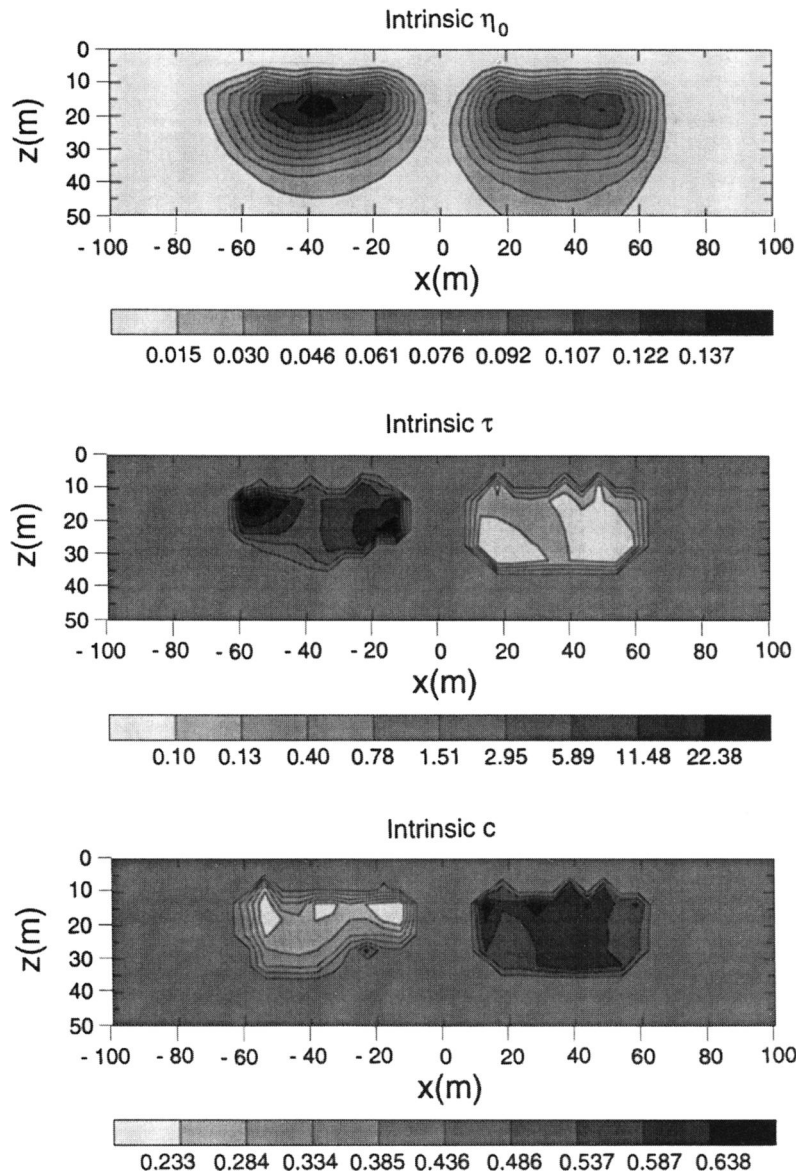


FIG. 6. The same results as shown in Figure 5, but thresholded so that only τ and c values corresponding to cells where $\eta_0 > 0.05$ are displayed.

a flatlying volcanic pile in the tropics. There are two kinds of polarizable bodies in the area. One is associated with sulfide mineralization, the other is associated with unmineralized clays from a hydrothermal alteration process.

The dc resistivity data and the chargeability data for the first time channel are shown in Figure 7. That figure also shows the conductivity and chargeability models obtained through inversion. Left of location 8900 are two polarized bodies at a depth of about 40 m. Their maximum chargeability is about 0.08, and their conductivity is less than 0.005 S/m. A lower chargeability zone concentrated closer to the surface is located to the right of 9205. The chargeability there does not exceed 0.02, and the conductivity ranges between 0.005 and 0.020 S/m. Figure 8 shows the pseudosections of apparent η_0 , τ , and c . The plots were smoothed in the horizontal direction by a 3-point averaging operator. The apparent η_0 in the upper panel of Figure 8 is higher on the left of the section and reaches 0.35. Lower η_0 values appear to the right of location 8970. The values on the right of the section vary but seem to be around 0.08, although a few exceed 0.1. The apparent τ values are plotted in the middle panel of Figure 8. Longer τ values, from 0.75 to 2 s, are associated with the higher chargeability bodies left of location 8970. Shorter and varying τ values, from 0.001 to 0.05 s, characterize the area right of 8970, although a few

longer τ values, up to 2 s, can be found around location 9500. The apparent c section shows a characteristic value of 0.3 in the left portion of the line associated with the higher η_0 and longer τ values. Smaller values ranging from 0.10 to 0.25 characterize the right portion, although a few values above 0.35 also can be found.

The 11 time channels of chargeability data were inverted to generate intrinsic decay curves. To eliminate unnecessary computation, only those curves whose first data point was greater than 0.011 were inverted to obtain the intrinsic η_0 , τ , and c . The resultant sections, smoothed in the horizontal and vertical directions by a 9-point averaging operator, are shown in Figure 9. The η_0 panel shows high values, exceeding 0.31, concentrated around locations 8600 and 8850 and at a depth of about 40 m. As seen in the two lower panels of Figure 9, the high chargeability is associated with τ values of about 1–3 s and c values of about 0.3. Most of the remaining η_0 model shows varying values between 0.08 to 0.15. Note that the difference in η_0 values between the left and right portions of the models are smaller than those on the chargeability model of the first time channel in Figure 7. Inspection of the τ model in Figure 9 reveals a surface layer characterized by long τ values of up to 6 s between locations 9300 and 9550. This layer is not pronounced in the conductivity or chargeability sections, but it seems to have

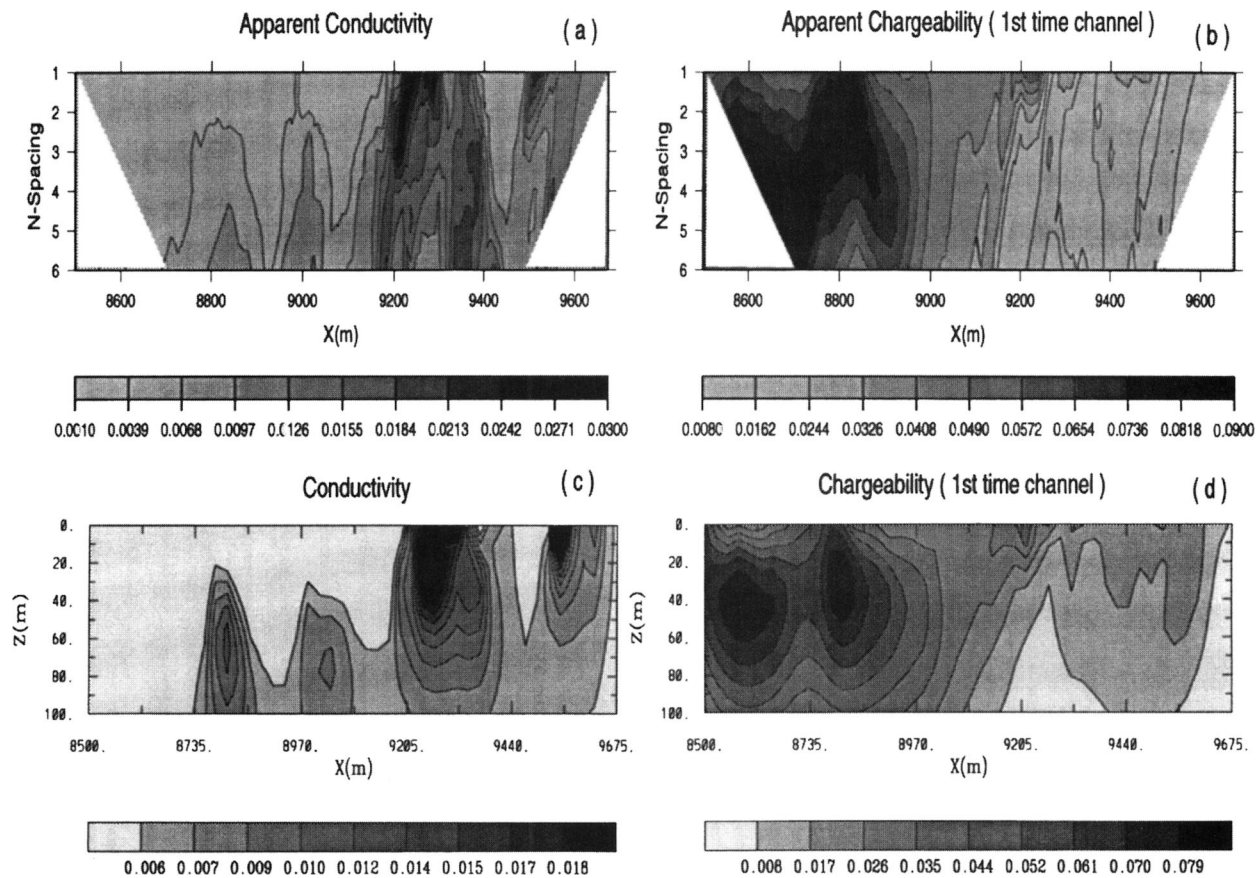


FIG. 7. The dc resistivity data (plotted as apparent conductivity), and apparent chargeability data for the first time channel are given in pseudosection form in (a) and (b), respectively. The conductivity obtained by inverting the dc resistivity data is shown in (c). Values are in S/m. The chargeability model, obtained by inverting the IP data, is shown in (d).

smaller c values than those at depth, and certainly smaller than the c values which characterize the two polarizable bodies on the left. The parts of the τ and c sections which are not associated with the two bodies on the left, or with the surface layer on the right, show varying short τ values in the range 0.003 to 0.3 s and c values between 0.15 and 0.35.

Our interpretation suggests that the two bodies left of location 8900 are sulfide mineralized bodies. Sulfide mineralization in the area is associated with silicification, which decreases the conductivity and contributes to the high chargeability. The expected τ value for sulfide mineralization is of the order of 0.1, but the rock texture may have a significant role in determining this parameter; our values, most of them around 1.0 s, are within a reasonable range. The chargeability in the right portion of the line has a different nature. The low chargeability

there, as seen in Figure 9, is almost negligible in models corresponding to data from later times (which are the ones usually considered), and could be attributed to some low-grade sulfide mineralization. Using the information in Figure 9, we surmise that the polarization in the right portion of the line is of significant value and has two different characters. The anomaly close to the surface, characterized by long τ and small c values, is thought to be associated with an alteration system. The varying short τ and larger c values below that layer are likely characteristic of the area and are seen also on the left above the two bodies.

DISCUSSION

The goal of this paper has been to make some headway into solving the problem of recovering Cole-Cole parameters from

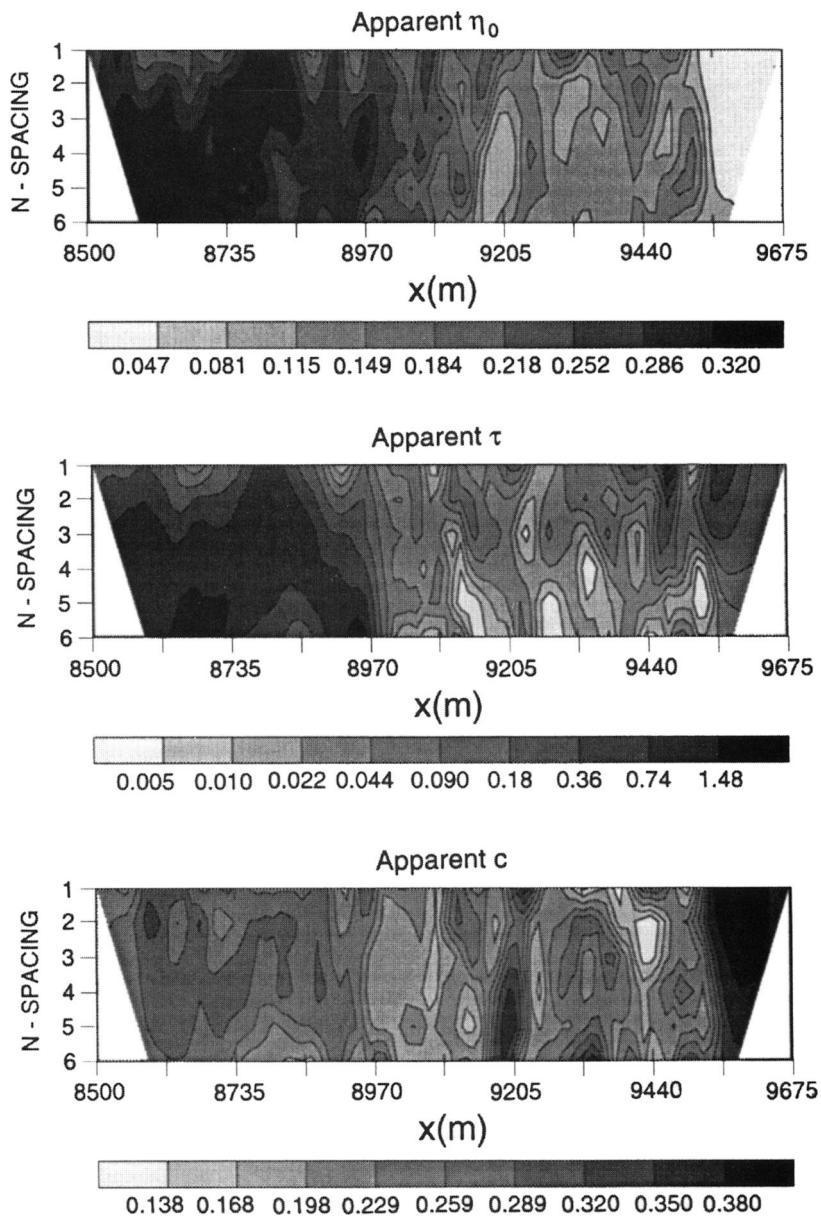


FIG. 8. Pseudosections of the Cole-Cole parameters obtained by inversion of the apparent decay curves.

time-domain IP data. Previous attempts to accomplish this centered around using a nonlinear parametric inversion of the apparent decay curves obtained from the field data. This approach can encounter difficulty in complex media because the apparent decay curves are really a mixture of intrinsic responses. In our paper, we treat the recovery of the Cole-Cole parameters as a two-step process. The first step is to unravel the mixing and to obtain an intrinsic decay curve for each earth cell. The second step focuses upon solving a nonlinear parametric inverse problem to recover the parameters for each decay curve.

Calculating the intrinsic decay curves is accomplished by inverting the IP data at each time channel to obtain an estimate of the chargeability distribution that corresponds to that time. It is essential that these inversions are consistent, and we have attempted to accomplish this by introducing a normalization procedure that quantifies how well each data set is to be misfit once

a reference channel (usually the first time channel of data) has been inverted. The two normalization procedures suggested both make use of the ratio of the norm of the observed data of the channel to be inverted to that of the reference channel. The application of this procedure to a synthetic example showed that our intrinsic decay curves are more representative of the true intrinsic decay curves than are the apparent decay curves.

The next step is to carry out a parametric inversion of the intrinsic decay curves to recover the Cole-Cole parameters. A variety of algorithms exist to do this. We have used a simulated annealing (SA) algorithm because of its intrinsic ability to avoid getting trapped in local minima. The application of SA inversion to the intrinsic decay curves from our synthetic model illustrated the advantages of our method compared to inverting apparent decay curves. We obtained sections of η_0 , τ ,

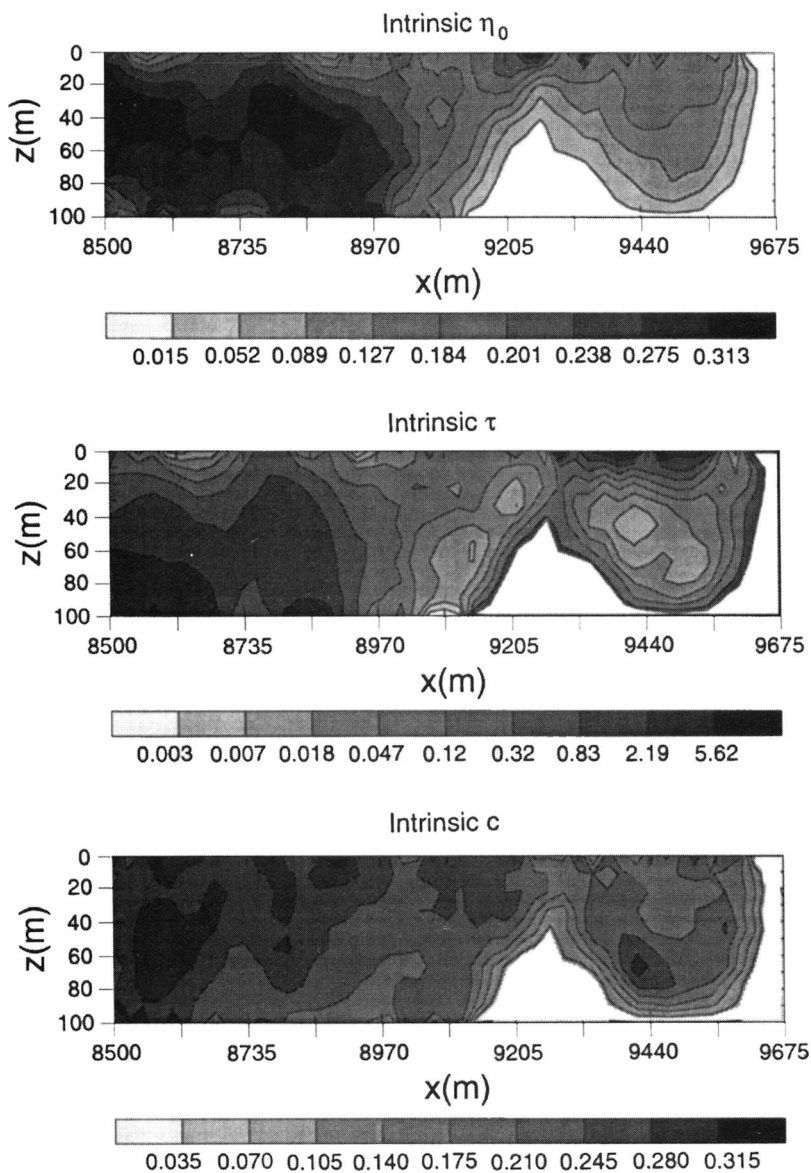


FIG. 9. The models of the Cole-Cole parameters obtained by inversion of the intrinsic curves. Only τ and c values corresponding to cells where $\eta_0 > 0.011$ are displayed.

and c which show the chargeable bodies in their approximate correct spatial positions rather than having pseudosections of these parameters and, additionally, the effects of mixing intrinsic responses are obviated. The application of our technique to a field data set suggested the existence of a geologic feature, seen on the τ section, which could not be seen on the chargeability section. This feature is in accordance with current thoughts about the geology in the region.

Despite the above successes, there is still a need for further research, especially regarding the parametric inversion of the intrinsic decay curves to recover the Cole-Cole parameters. Selection of a misfit criterion is one issue that needs to be explored further. Most importantly, the inversion results are nonunique, and an investigation of the limitation of the parametric inversion algorithm in recovering accurate values of the parameters is required. Further regularization to produce smoother 2-D sections of the Cole-Cole parameters is also desirable. All of the investigations on nonuniqueness must be linked to the choice of pulse train current used in the field survey. Nevertheless, the results we have obtained are encouraging and lead us to believe that more complete representations of Cole-Cole parameter sections can be computed. These, in turn, may be useful in helping to differentiate different geologic units.

ACKNOWLEDGMENTS

We thank Peter Kowalczyk and Placer Dome for supplying the field data set and for discussions concerning its interpretation. This work was supported by an industry consortium, Joint and Cooperative Inversion of Geophysical and Geological Data. Participating companies are Placer Dome, BHP Minerals, Noranda Exploration, Cominco Exploration, Falconbridge

Limited (Exploration), INCO Exploration and Technical Services, Hudson Bay Exploration and Development, Kennecott Exploration, Newmont Gold Company, WMC, and CRA Exploration. We thank Partha Routh for supplying the VFSA code and Yaoguo Li for numerous helpful discussions. We also thank W. Pelton, W. Frangos, and R. Sigal for reviewing this manuscript and for their helpful suggestions.

REFERENCES

- Guptasarma, D., 1982, Computation of the time-domain response of a polarizable ground: *Geophysics*, **47**, 1574–1576.
- Ingber, L., 1989, Very fast simulated reannealing: *Math. Comput. Modeling*, **12**, 967–993.
- Johnson, J. M., 1990, Spectral IP parameters derived from time-domain measurements, *in* Fink, J. B., McAlister, E. O., Sternberg, B. K., Widuwilt, W. G., and Ward, S. H., Eds., *Induced polarization: Applications and case histories*, Soc. Expl. Geophys.
- Kirkpatrick, S., Gelatt, C. D., Jr., and Vecchi, M. P., 1983, Optimization by simulated annealing: *Science*, **220**, 671–680.
- Madden, T. R., and Cantwell, T., 1967, Induced polarization, a review, *in* *Mining Geophysics, 2, Theory*: Soc. Expl. Geophys., **46**, 916–931.
- Metropolis, N., Rosenbluth, A., Rosenbluth, M., Teller, A., and Teller, E., 1953, Equation of state calculations by fast computing machines: *J. Chem. Phys.*, **21**, 1087–1092.
- Oldenburg, D. W., and Li, Y., 1994, Inversion of induced polarization data: *Geophysics*, **59**, 1327–1341.
- Pelton, S. H., Ward, S. H., Hallof, P. G., Sill, W. R., and Nelson, P. H., 1978, Mineral discrimination and removal of inductive coupling with multifrequency IP: *Geophysics*, **43**, 588–609.
- Press, W. H., Teukolsky, S. A., Vetterling, W. T., and Flannery, B. P., 1992, *Numerical recipes*, Cambridge Univ. Press.
- Siegel, H. O., 1959, Mathematical formulation and type curves for induced polarization: *Geophysics*, **24**, 547–565.
- Soininen, H., 1985, The behavior of the apparent resistivity phase spectrum in the case of two polarizable media: *Geophysics*, **50**, 810–819.
- van Laarhoven, P. J. M., and Aarts, E. H. L., 1988, *Simulated annealing: Theory and applications*: Kluwer Academic Publishers.
- Zonge, K. L., and Wynn, J. C., 1975, Recent advances and applications in complex resistivity measurements: *Geophysics*, **40**, 851–864.